Surface Energy Balance Algorithm for Land (SEBAL) based Evapotranspiration Estimation in Lower Gilgel Abay Catchment Lake Tana Sub-Basin, Ethiopia

Tewodros Kassaye Semaw[1], Sirak Tekleab[2], Marco Napoli[3]

[1]Organization for Rehabilitation and Development in Amhara (ORDA), *E-mail: teddyk2004@gmail.com*, P.O. Box 132, Bahir Dar, Ethiopia.
[2] Hawassa University, Institute of Technology, Department of Water Resources and Irrigation Engineering. P.O Box 5, *E-mail: sirakteklеab@yahoo.com*, Hawassa, Ethiopia.
[3]DISPAA Department of Agri-food Production and Environmental Sciences, University of Florence, Piazzale delle Cascine18 50144, Firenze (Italy). *E-mail: marco.napoli@unifi.it*.

Abstract
On land, Evapotranspiration (ET) plays an important role in the water cycle and is an important parameter in water resources management. Remote sensing is one of the important sources of data and techniques to estimate many climate elements including evapotranspiration. The estimation based on remote sensing is vital for the management of water resources in the catchment. This study estimated the spatio-temporal variation of evapotranspiration in the lower Gilgel Abay catchment, Lake Tana sub-basin from January to March 2016. The evapotranspiration was quantified using the Surface Energy Balance (SEBAL) algorithm and Landsat 8 imagery with climate data. For this analysis, ASTER GDEM, GRASS-python & reference weather parameters from Bahir Dar weather station were used. Parameters including surface radiance, surface reflectance, surface albedo, NDVI, LAI, surface emissivity, surface temperature, net radiation, soil heat flux, sensible heat flux, and latent heat flux were computed. Consequently, the hourly, daily, monthly and seasonal evapotranspiration in the study area were calculated with SEBAL python. The pixel wise calculation shows that the values of the spatial variation of mean ET varied from 0 mm/day to 7.39 mm/day with a mean value of 4.78 mm/day for 23 December 2016. The computed ET values for the months December to March, the maximum estimated ET over the whole catchment ranged from 6.51 mm/day to 7.82 mm/day. The mean ET ranged from 4.37 mm/day to 4.78 mm/day while the seasonal ET was 539.92 mm for 2016. ET values were computed for different conventional methods using REF-ET software. The value of Standard P-M for the weather station was used as a reference to compare the values obtained from other conventional methods as well as SEBAL method. The mean value of the study area from SEBAL calculation approached the point values of CIMIS penman, standard P-M and Priestly Taylor methods. The analyses are vital from the perspective of water resources management on various surfaces of the earth that need to be understood to achieve sustainable development of water resources in the basin and recommended to apply in the remaining sub-basins in the region.

Keywords: Evapotranspiration, Gilgel Abay, GRASS-GIS, Landsat-8, RS, SEBAL.

***Corresponding author's address**: Tewodros Kassaye email <*teddyk2004@gmail.com*>. Tel: +251-912420028/+251-923650635.

INTRODUCTION
The ability to predict evapotranspiration (ET) levels is a valuable asset to manage water resources. ET is a good indicator of the effectiveness of irrigation and the total water consumption of vegetation. Evapotranspiration information is useful for irrigation supply planning, regulation of water rights, and watershed studies (Waters, et al., 2002). ET is important in predicting soil water availability, flood forecasting, rainfall forecasting, and projecting changes in occurring heat waves and droughts (Merlin, et al., 2014). With the use of remote sensing, it is possible to directly derive the water consumed as ET without the need to quantify other complex hydrological processes (Trezza, et al., 2013).

Accurate estimation of ET plays an important role in the quantification of the water balance at the level of basin, river basin, and regional scale for better planning and management of water resources. Accurate quantification of ET in irrigated agriculture is crucial to optimize crop production, water distribution planning, irrigation management, assessment of the effects of land-use change on water yields, development of best practices of management to minimize the degradation of surface and groundwater and assessment of land use and practices of water resources management and environmental quality (Irmak, et al., 2006a; 2006b). Several methods are available to estimate ET: Bowen Ratio energy balance (BREBS) systems, weighing lysimeters, and water balance techniques offer powerful alternatives for measuring ET and

other energy flows on the surface. Despite the elegance, high precision, and theoretical attractions of these techniques for measuring ET, their practical use in large areas could be limited.
Agriculture is the backbone of the Ethiopian economy. Therefore, to maximize agricultural production for domestic use and to complement the industry's leading economy, irrigation is the non-alternative option. Hence, wise use of limited water resources, reliable maps of surface energy fluxes for assessing surface-atmosphere interaction and knowledge, and proper quantification of evapotranspiration are important to maximize production with better irrigation management practices.

The evaporation flux was commonly estimated through hydrological models. ET is highly variable in both space and time due to the wide spatial variability of precipitation, hydraulic characteristics of soils, and vegetation types and densities. It is variable in time due to the variability of climate. Satellite images provide an excellent means for determining and mapping the spatial and temporal structure of ET. The estimation of evapotranspiration using remote sensing-based approaches is largely unexplored research in the study area.

Therefore, to overcome this problem, satellite-based evapotranspiration estimation was employed in the lower part of Gilgel Abay catchment, Lake Tana sub-basin. The catchment contributes much of the water into the Lake Tana. Consequently, the evapotranspiration estimation is vital from the perspective of accurate water balance of the Lake Tana and water resources planning in the catchment. The main objective of this study was, therefore, to estimate evapotranspiration using Surface Energy Balance Algorithm for Land /SEBAL and landsat-8 data using SEBAL-python and GRASS-GIS. Consequently, it enables us to know the amount of water used by the evapotranspiration process over specified months in the catchment.

STUDY AREA

The lower part of Gilgel Abay catchment is located in the Northwest highlands of Ethiopia between 259026.33 m to 311468.19 m N latitude and 1256107.36 m to 1306929.16 m E longitudes (
Figure 1). The study area covers a total area of 1,743.47 km^2 upstream of Lake Tana. The Gilgel Abay River is contributing about 60% of the inflow into Lake Tana. (Tessema, 2006).

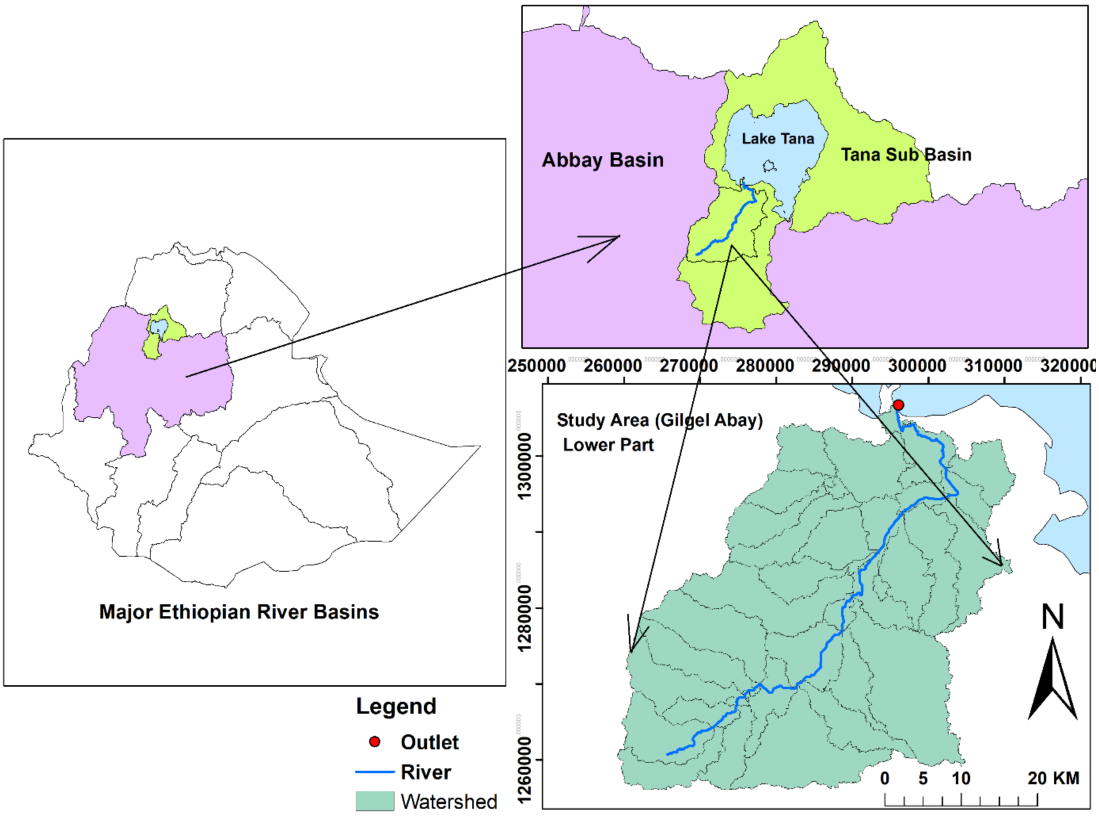

Figure 1. Location Map of the Study area

The elevation of Lower Gilgel Abay catchment varies from 1699 to 2667 m a.s.l. The slope map of the study area was derived from DEM and varies from 0 to 50%. In general, the annual average temperature of the Gilgel Abay basin falls in the range of 16 ^{0}C to 20 ^{0}C (Kebede, 2009). Based on BCEOM (1998) the dominant soil type is Halpic Luvisol which covers 37.52%.

MATERIALS AND METHODS

To estimate ET cloud-free Landsat 8 scene (LS8 - OLI/TIRS) including MTL file for Dec 23, Jan 22, Feb 07, and Mar 10/2016 with Path: 170 and Row: 52 and reflectance of each band, Digital Elevation Model (DEM) from ASTER UTM format, Re projected the DEM and renamed to MDT_Sebal.TIF, shape file of the study area and SEBAL_GRASS-Master file all were organized in the same datasets to run the algorithm. The land use/cover classification was derived from www.geoportal.rcmrd.org and nine land-use types were identified for the study area. Annual cropland use types occupy the largest percentage of the study area (more than 88%). The accuracy of the classified map was validated by different techniques like ERDAS Imagine with google earth, QGIS with open layer plugins (google satellite, google hybrid, and Google Street), and google earth tools. The SEBAL algorithm (Bastiaanssen, et al, 1998; 2005) was used to compute the evapotranspiration.

Atmospheric correction models to calculate reflectance, surface albedo, emissivity, surface temperature and elements of the solar radiation balance, including net radiation, soil heat flux, sensitive heat flow, latent heat flow, and finally calculate instantaneous and daily evapotranspiration values were calculated using GRASS-GIS software with the help of GRASS-python file developed by Wagner (2017). The methodological framework used in the research is provided in Fig. 2.

SEBAL MODEL

In the SEBAL model, ET was computed from satellite images and weather data using the surface energy balance equation. Since the satellite image provides information for the overpass time only, SEBAL computes an instantaneous ET flux for this overpass time. The ET flux was, then, calculated for each of the pixels of the image as a “residual” of the surface energy budget equation:

$$\lambda ET = R_n - G - H \text{ ------------------------------ (1)}$$

Where: λ ET is an instantaneous value (latent heat flux) for the time of the satellite overpass (W/m^2). Rn is the net radiation flux at the surface (W/m^2), G is the soil heat flux (W/m^2), and H is the sensible heat flux to the air (W/m^2).

The net radiation flux at the surface (Rn) represents the actual radiant energy available at the surface. It was computed by subtracting all outgoing radiant fluxes from all incoming radiant fluxes. This is given in the surface radiation balance equation:

$$Rn = RS{\downarrow} - \alpha\, RS{\downarrow} + RL{\downarrow} - RL{\uparrow} - (1-\varepsilon o)\, RL{\downarrow} \text{------(2)}$$

RS↓ is the incoming shortwave radiation (W/m2), α is the surface albedo (dimensionless), RL↓ is the incoming longwave radiation (W/m^2), RL↑ is the outgoing longwave radiation (W/m^2), and εois the surface thermal emissivity (dimensionless).

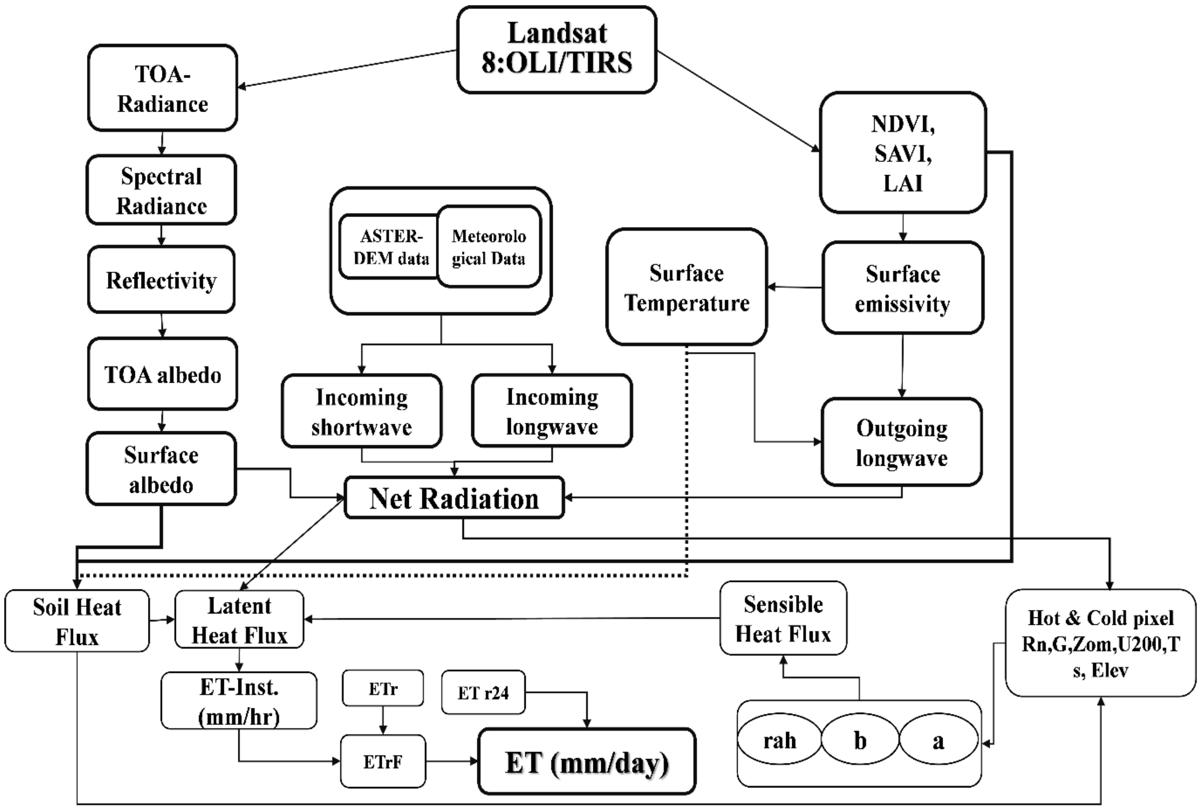

Figure 2. General methodological flow chart

Calculation of Surface Radiation elements

The net surface radiation flux (Rn) was computed using the surface radiation balance equation. Atmospheric correction for solar radiation elements is important in remote sensing analysis; its necessity depends on the objectives of the analysis. The analysis of this study was carried out using semi-automatic classification plugin /SCP/ in QGIS software.

Surface albedo was computed by the equations mentioned in Tasumi, et al. (2008) and shown below.

$$\alpha = \frac{\alpha_{TOA} - \alpha_{Path\_radiance}}{\tau_{sw}^{2}} \text{ --------------------(3)}$$

Where; *αpath_radiance* is the average portion of the incoming solar radiation across all bands that is backscattered to the satellite before it reaches the earth's surface, and ranged from 0.025 to 0.04 in SEBAL and 0.03 is recommended.

τsw is shortwave atmospheric transmissivity and calculated using the equation

$$\tau_{sw} = 0.75 + 2\times10^{-5} \times z \text{ --------------------------- (4)}$$

Where z is an elevation of an area defined by ASTER GDEM Data (MDT_Sebal).

Vegetation indices

Three commonly used vegetation indices (NDVI, LAI, and SAVI) were computed using the reflectivity values in GRASS-SEBAL. Those indices were used to calculate the outgoing longwave radiation through a function of surface temperature and land surface emissivity.

Normalized Difference Vegetation Index (NDVI), and Leaf Area Index (LAI) were calculated by visible and near-infrared bands (Waters, et al., 2002; Lillesand, et al., 2004). For Landsat-8, NDVI is a sensitive indicator of the amount and condition of green vegetation. Values for NDVI range between -1 and +1. Green surfaces have NDVI between 0 and 1 and water and cloud are usually less than zero.

$$NDVI = \left(\frac{NIR - RED}{NIR + RED}\right) \text{ ---------------------------(5)}$$

Soil adjustment Vegetation Index (SAVI) is an index that attempts to "subtract" the effects of background soil from NDVI so that impacts of soil wetness are reduced in the index. It is computed as (Waters, et al, 2002).

$$SAVI = \left(\frac{(1+L)(NIR - RED)}{L + NIR + RED} \right) \text{------------------ (6)}$$

Where; L is a constant for SAVI. If L is zero, SAVI becomes equal to NDVI. A value of 0.5 frequently appears in the literature for L (Waters, et al, 2002).
Leaf Area Index (LAI), the ratio of the total area of all leaves on a plant to the ground area represented by the plant, was computed following the empirical equation by Weng, et al. (2004).

$$LAI = -\ln \frac{\left(\frac{0.69 - SAVI}{0.59} \right)}{0.91} \text{------------------------ (7)}$$

Emissivity and land surface temperature

Both surface emissivity (broadband and narrowband) were used for the calculation of the total longwave radiation emitted from the surface and surface temperature respectively.

The values of emissivity were estimated from NDVI and LAI as follows:

$$\varepsilon = 1.009 + 0.047 \times \ln(NDVI) \text{--------------(8)}$$

Where NDVI > 0, otherwise, emissivity is assumed zero (e.g. water)
Narrow band emissivity was computed using the following empirical equation.

$$\varepsilon NB = 0.97 + 0.0033 \times LAI \text{ ------------------------ (9)}$$

ε0 = 0.95 + 0.01 x LAI ------------------------------ (10)

Where LAI < 3,
When LAI >= 3; ε (emissivity) = 0.98 (Kosa, 2011; Opoku et al., 2008).
For water, NDVI < 0 and surface albedo < 0.47, ε0 = 0.985 and εNB = 0.99 (Waters, et al., 2002)
For snow, NDVI < 0 and surface albedo >= 0.47, ε0 = 0.985 and εNB = 0.99 (Waters, et al., 2002)

For this calculation, NDVI, LAI, and surface albedo are input parameters to compute emissivity in both cases. Hence, computation is done using GRASS-GIS SEBAL python.

The black body temperature was corrected with respect to the surface emissivity (ε) values to compute the land surface temperature (Ts) using the formula given by Weng, et al., (2004).

$$Ts = \frac{Tb}{1 + (\lambda \times Tb / \gamma) \times \ln \varepsilon NB} \text{ ------------------ (11)}$$

Where: **λ** is the average of limiting wavelengths of band 10 of Landsat8-TIRS (10.8)

$$\gamma = h \times c / a(0.01438 m.K) \text{ ------------ (12)}$$

γ = 14380
a = Boltzmann constant (1.38x10-23j.k)
h = Plank’s constant (6.626x10-34 J.s)
c = velocity of light (2.998 x 108 m/s)

Calculation of Solar Radiations Elements and ET

The solar radiation and ET were computed following the procedure set by (Bastiaanssen, et al., 1998).
Incoming shortwave radiation (RS↓) (W/m^2) was calculated using the available climatic parameters (sunshine hours, relative humidity, minimum and maximum temperature cloud cover, and geographic location), the solar constant, the solar incidence angle, a relative earth-sun distance, and the calculated atmospheric transmissivity. It is calculated, assuming clear sky conditions, as a constant for the image time (Waters, et al., 2002; Chiemeka, 2008) using:

$$Rs \downarrow = G_{Sc} \times \cos\theta \times d_r \times \tau_{sw} \text{ ---------------- (13)}$$

Where GScis solar constant (1,367 W/m^2), θ is the solar incidence angle, = sun elevation angle, given in the header data file of the landsat-8 imagery, *dr*= the inverse squared relative earth-sun distance, and is the atmospheric transmissivity.

The outgoing longwave radiation (RL↑) was computed at each pixel using the Stefan-Boltzmann equation (W/m^2) (Eq. 14) with a calculated surface emissivity and surface temperature (Waters, et al., 2002; Opoku Duah, et al., 2008). This calculation is done using GRASS-GIS SEBAL Python.

$$RL \uparrow = \varepsilon 0 \times \sigma \times Ts^4 \text{ -------------------- (14)}$$

Where **ε0** is the broadband surface emissivity, **σ** is Stefan-Boltzmann constant (5.67 x 10-8 W/ m^2/ K4) and Ts is surface temperature in K.

The incoming longwave radiation (RL↓), the downward thermal radiation flux from the atmosphere (W/m^2), was computed using a modified Stefan-Boltzmann equation with atmospheric transmissivity and a selected surface reference temperature. To compute this radiation (*RL*↓), the hot and cold pixels were selected as anchor pixels and are located in the area of interest. The "cold" pixel was selected as a wet, well-irrigated crop surface having full ground cover by vegetation whereas the "hot" pixel was selected as a dry, bare agricultural field where ET is assumed to be zero.

Using surface albedo (α), outgoing longwave radiation (RL↑), and broadband surface emissivity (ε0) along with the incoming shortwave radiation (RS↓) and the incoming longwave radiation (RL↓), net radiation flux was calculated.

Calculation of surface energy budget elements

Soil heat flux (G) and sensible heat flux (H) were computed in SEBAL using the surface energy budget equation. Soil heat flux (G) is the rate of heat storage in the soil because of the temperature gradient between the soil surface and the underlying upper layers of the soil (W/m^2) (Opoku Duah, et al., 2008; Waters, et al., 2002; Tasumi, et al., 2003). It is calculated using the equation given below:

$$G/R_n = T_s/\alpha(0.0038\alpha + 0.0074\alpha^2)(1-0.98NDVI \quad \text{----(15)}$$

Where;
Ts is the surface temperature (^{0}C),
α is the surface albedo, and
NDVI is the Normalized Difference Vegetation Index.
G is then readily calculated by multiplying G/Rn by the value for Rn computed in the above equation.

The ratio of G/Rn was assigned equal to 0.5 for the condition of NDVI < 0; Ts< 4 ^{0}C and α > 0.45. The resulting image was converted to soil heat flux (G) in W/m2 by multiplying the ratio G/Rn by Rn. (Waters, et al., 2002).

Sensible Heat Flux (H) is the rate of heat loss to the air by convection and conduction, due to temperature gradients (Morse, et al., 2001) and (Oberg and Meless, 2006). It was computed using the following equation:

$$H = (\rho \times c_p \times dT)/r_{ah} \quad \text{------------------------- (16)}$$

Where: **H** is sensible heat flux, **ρ** is air density (kg/m^3), *C*p is air specific heat (1004 J/kg/K), dT is near surface temperature differences (T_1-T_2) in K between two heights (Z_1 & Z_2) above the zero plane displacement, and ***rah*** is aerodynamic resistance to heat transport (s/m).

Latent heat flux is the rate of latent heat loss from the surface due to evapotranspiration (Waters, et al., 2002). It was computed for each pixel using Equation (17)

$$\lambda ET = R_n - G - H \quad \text{--------------------------- (17)}$$

Where: λ ET is an instantaneous value for the time of the satellite overpass (W/m^2).
Instantaneous value of ET in equivalent evaporation depth was computed as:

$$ET_{inst} = 3600 \times \frac{\lambda ET}{\lambda} \quad \text{--------------------------- (18)}$$

Where: ET*inst* is the instantaneous ET (mm/hr), 3600 is the time conversion from seconds to hours, and λ is the latent heat of vaporization or the heat absorbed when a kilogram of water evaporates (J/kg).

After calculating latent heat flux (λ), ETinst (mm/hr) and reference ET fraction (ETrF) were calculated simultaneously at each pixel level for the image time (ETr & U @10:52:11 local time). Once the Instantaneous ET (ETinst) and Reference ET Fraction (ETrF) were developed, daily evapotranspiration calculation was made using Equation (19).

$$ETrF = \frac{ET_{inst}}{ET_r} \quad \text{------------------------------- (19)}$$

Where, ETinst is instantaneous ET (mm/hr) and ETr is the reference ET at the time of the image from the REF-ET software (mm/hr) developed by the University of Idaho (Allen, 2000). ETrF is similar to the well-known crop coefficient; Kc. ETrF was used to extrapolate ET from image time to periods of 24 hours or more.

ETr was used in SEBAL to estimate the ET at the "cold" pixel and to calculate the reference ET fraction (ETrF) and ETr was computed for a given weather station using the REF-ET software (Allen. 2000).

Daily values of ET (ET24) were often more useful than instantaneous ET. SEBAL computes the ET24 by assuming that the instantaneous ETrF computed in the model is the same as the 24-hour average. Finally, the ET24 (mm/day) was computed as:

$$ET_{24} = ETrF \times ET_{r\_24} \text{ ------------------------ } (20)$$

Where, ETr-24 is the cumulative 24-hour ETr for the day of the image (Waters, et al., 2002). This is calculated by adding the hourly ETr values over the day of the image.

$$ET_{r\_24} = \sum_{h}^{24} ET_{r-h} \text{ --------------------------- } (21)$$

The evapotranspiration map that covers a season/month of full growth was derived from the 24-hour evapotranspiration data by extrapolating the ET24 proportionally to the reference evapotranspiration (ETr).

RESULTS AND DISCUSSION

The majority of the study area (more than 88%) came under annual cropland use types (Figure 3).

The surface albedo value was lower for the water body having an average value (0.106) recognized due to high absorption properties (Fig. 4), while the settlement with the highest average value (0.194) was recognized because of the low absorption and scattering from such land cover types. According to Ayad et al., (2016), surface albedo having high absorption properties (forest, grass, and water body) are recognized with low average values of 0.05 to 0.08 while, surface albedo having low absorption properties (bare land and rock outcrop) are recognized with highest average values of 0.18 and 0.17, respectively.

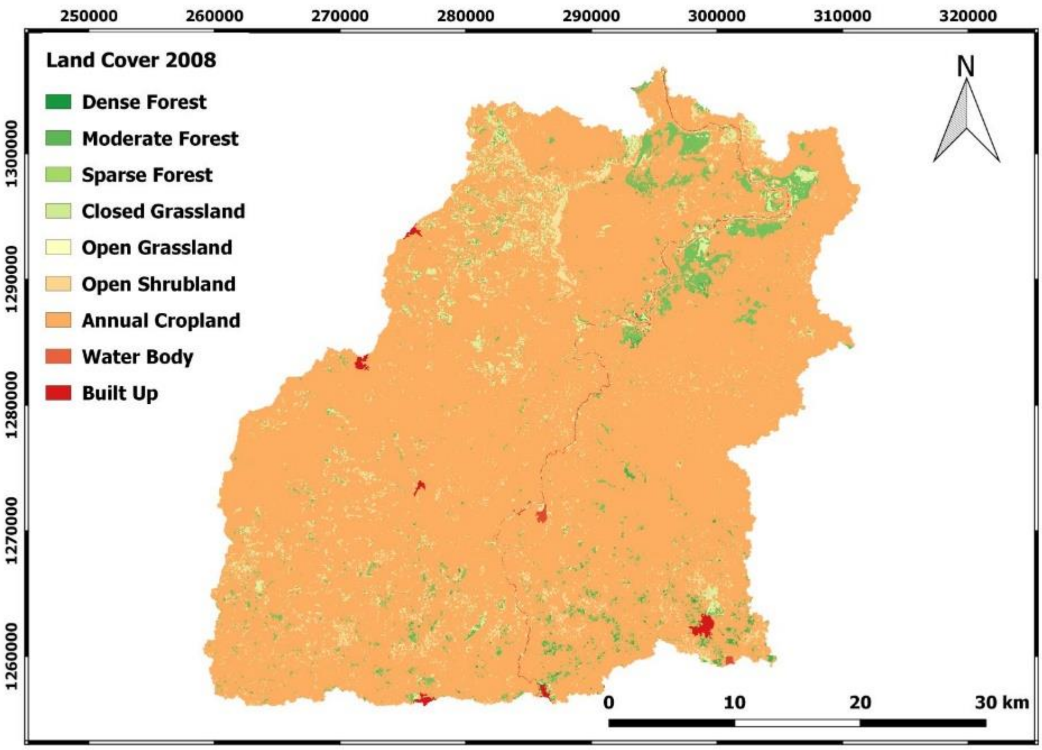

Figure 3. Land Use Map of the study area (Source: RCMRD (2015))

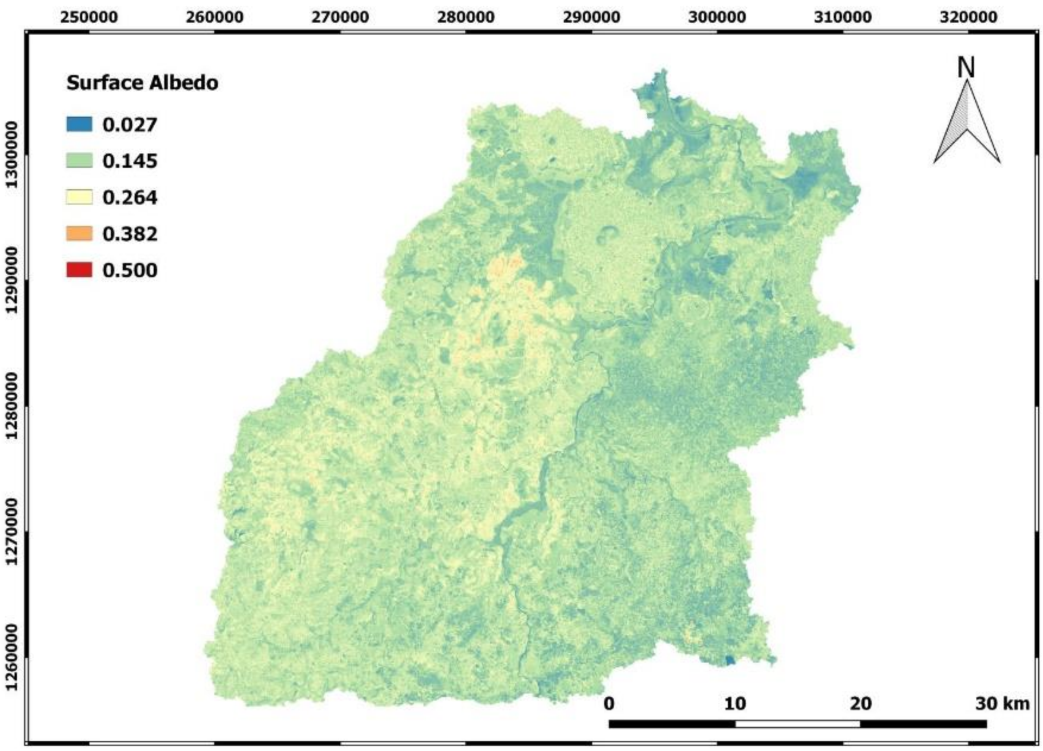

Figure 4. Map of Surface albedo

The NDVI values of the computed spatial variation ranged from -0.90 to 0.85 (Fig. 5). The NDVI mean value of the water body was low (0.12), whereas 4.37% of the area coverage (forest) showed high NDVI with the mean value of 0.61. The areas along with the closed grassland represent low LAI (Fig. 6) of the mean value 0.12, whereas 4.37% of the area coverage (forest) showed high LAI with the mean value of 0.68. According to Jana, et al., (2016) the areas along with the river (water body) represent a low vegetation index of ranges from 0.14 to 0.22 whereas, forest areas showing high vegetation density recognized by higher average values of NDVI ranges from 0.6 to 0.65.

Using the radiant temperature and the computed value of surface emissivity (narrowband surface emissivity εNB), the surface temperature (K) map was derived. Figure 7 clearly showed the dependence of the Surface Temperature estimation on the surface albedo and the vegetation. Variations in the mean temperature values were low and ranged from 28.23 ^{0}C in forest area and water body due to high absorption properties (lower surface albedo and higher NDVI) to 33.28 ^{0}C for the other land cover types (Fig. 8).

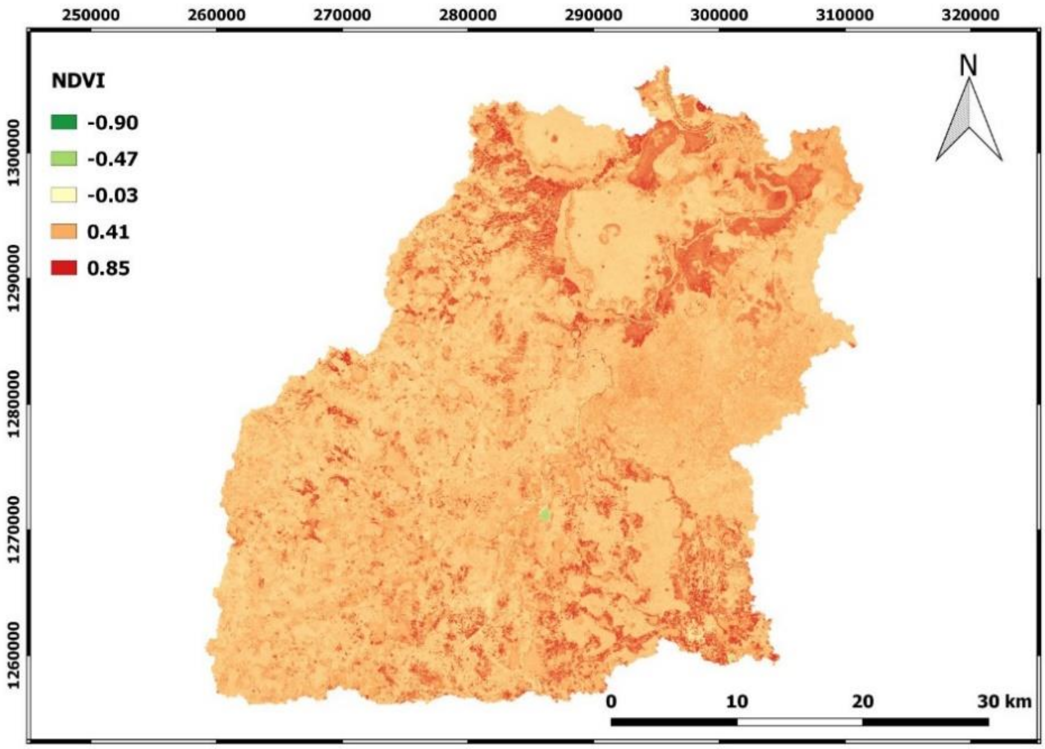

Figure 5 Map of Normalized Difference Vegetation Index

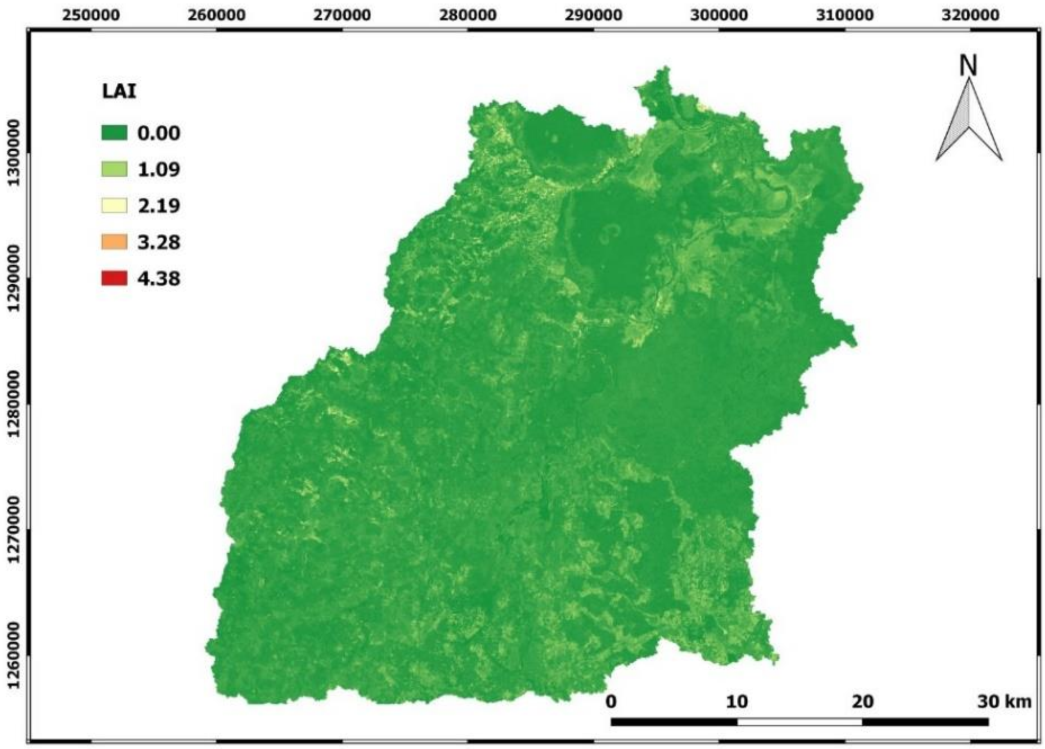

Figure 6. Map of Leaf Area Index

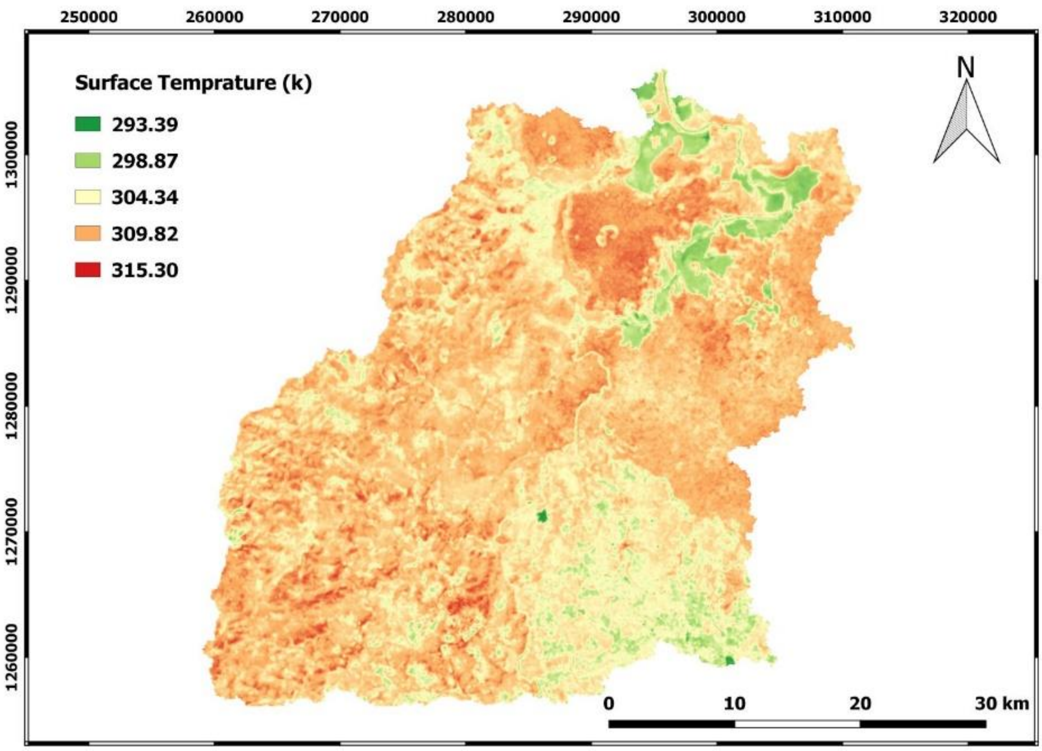

Figure 7. Land surface temperature (^{0}K)

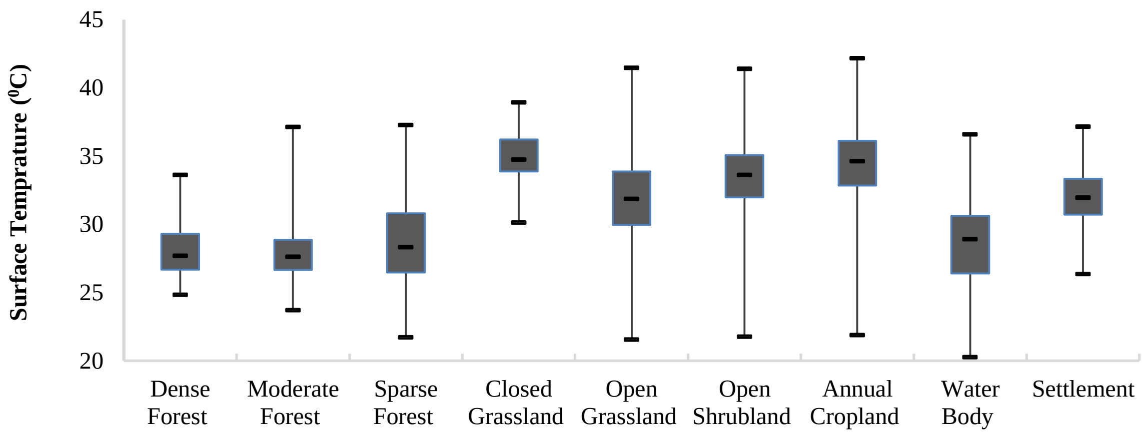

Figure 8. Mean surface temperature for land covers.

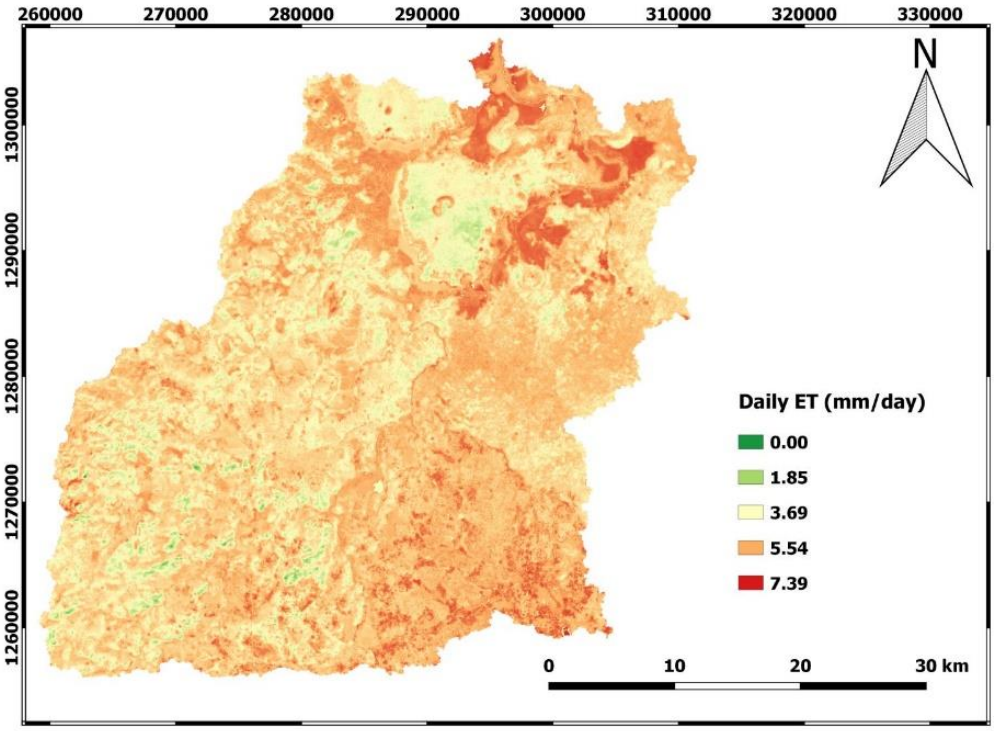

Figure 9. Map of Daily Evapotranspiration

Table 1: Daily evapotranspiration (mm/day) distribution for different land cover type

Land Cover Type	Area (km^2)	%	Daily ET (mm/day)				
			Min	Max	Range	Mean	STD
Dense Forest	0.22	0.01	4.82	7.00	2.18	6.25	0.38
Moderate Forest	6.33	0.37	0.64	7.09	6.45	6.23	0.46
Sparse Forest	68.41	3.99	1.14	7.00	5.86	5.97	0.50
Closed Grassland	0.51	0.03	2.51	5.89	3.38	4.42	0.50
Open Grassland	49.43	2.88	0.63	7.17	6.55	5.42	0.77
Open Shrub land	61.67	3.60	0.27	6.81	6.54	4.96	0.62
Annual Cropland	1,516.57	88.49	0.00	7.09	7.09	4.69	0.73
Water Body	5.99	0.35	3.25	7.39	4.14	5.13	1.15
Settlement	4.72	0.28	3.17	6.69	3.52	5.20	0.51

The daily evapotranspiration value ranged from 0 to 7.39 mm/day, and a mean value of 4.78 mm/day (Fig. 9). The computed daily ET values for each land use type showed that forest land use exhibit the largest ET with a mean value of 6.25 mm/d as compared to the grassland with a mean value of 4.42 mm/d (Table 1). These findings are in line with studies conducted in the Rift Valley Lakes basin and Lake Tana sub-basin (Ayenew, 2003; Temesgen, 2009; Muhammed, 2012; Mulugeta et al., 2017).

During satellite overpass time, the variation of ET in mm/day in relation to NDVI and surface temperature in ^{0}C, water body had a high surface temperature of about 28.10 ^{0}C and the estimated ET from the same land use was mainly contributed from evaporation, which was about 5.13 mm/day (Figure **10**.10). On the other hand, the forest area showed an average surface temperature of 28.27 ^{0}C with high vegetation index (0.61) and a mean ET value of 6.15 mm/day.

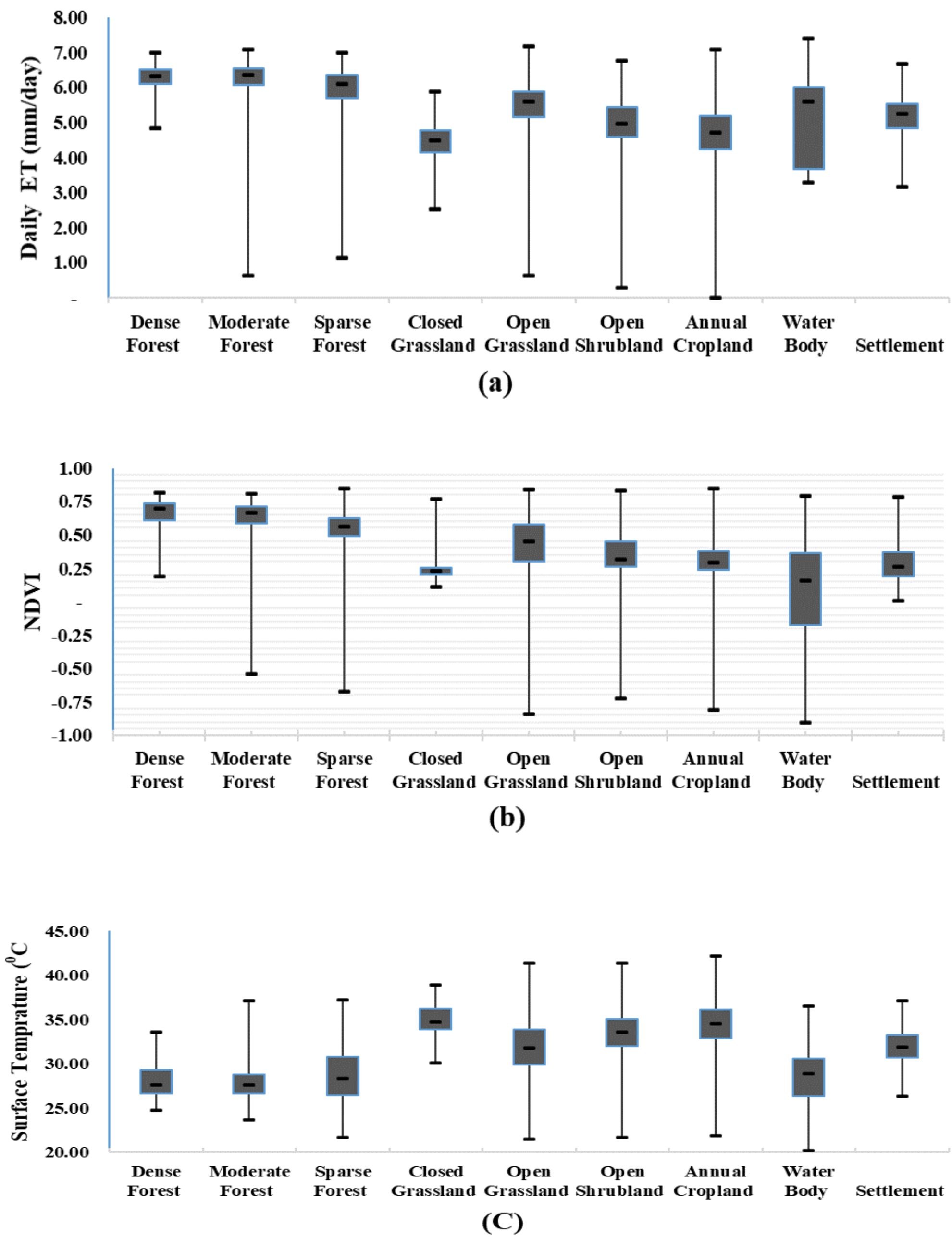

Figure 10. Comparison between ET (a), NDVI (b) ST (c) during satellite overpass time.

The maximum estimated actual evapotranspiration over the whole catchment ranged from 6.51 mm/day (Jan) to 7.82 mm/day (Mar) (Figure 11). The mean actual evapotranspiration ranged from 4.37 mm/day (Feb) to 4.78 mm/day (Dec). Daily ET was nearly the same as the average ET in annual cropland (88.49%), higher in the forestland cover types and lower in closed grassland cover type (Figure 11).

Figure12 showed the trend of daily ET for each month in different land cover types. Forestland cover types higher in December and January than in February and March due to higher NDVI and lower surface temperature during those months.

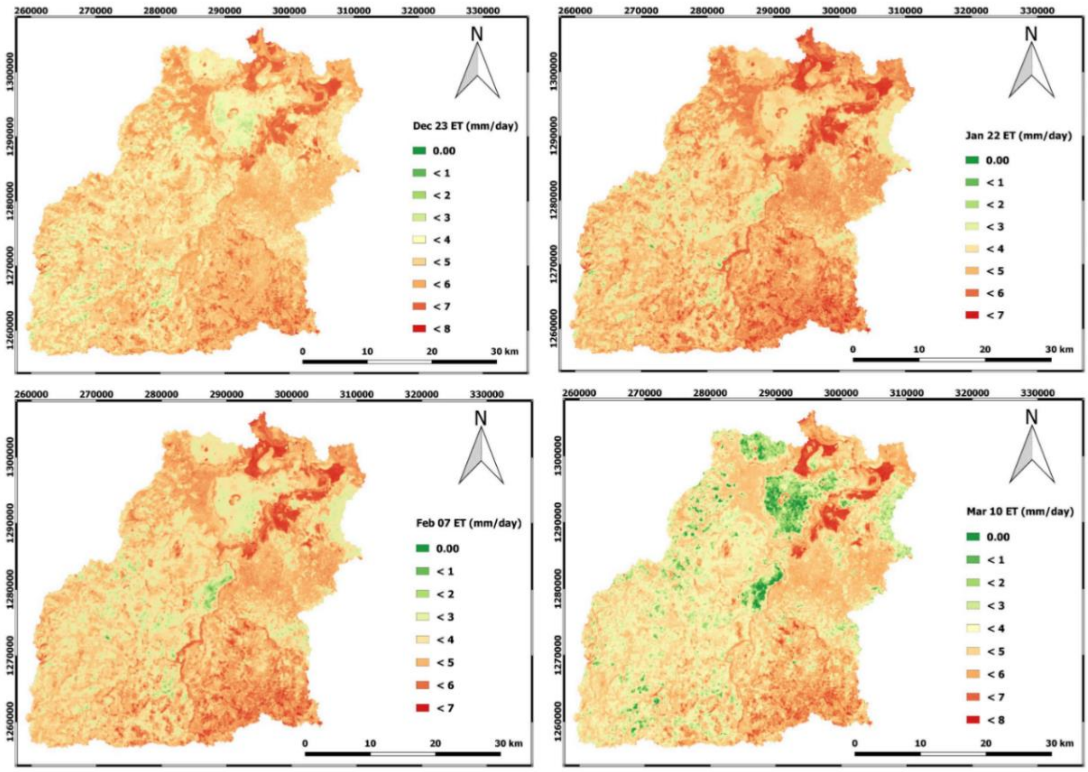

Figure 11. Map of Twenty-Four-hour evapotranspiration for four months (Dec to March 2016)

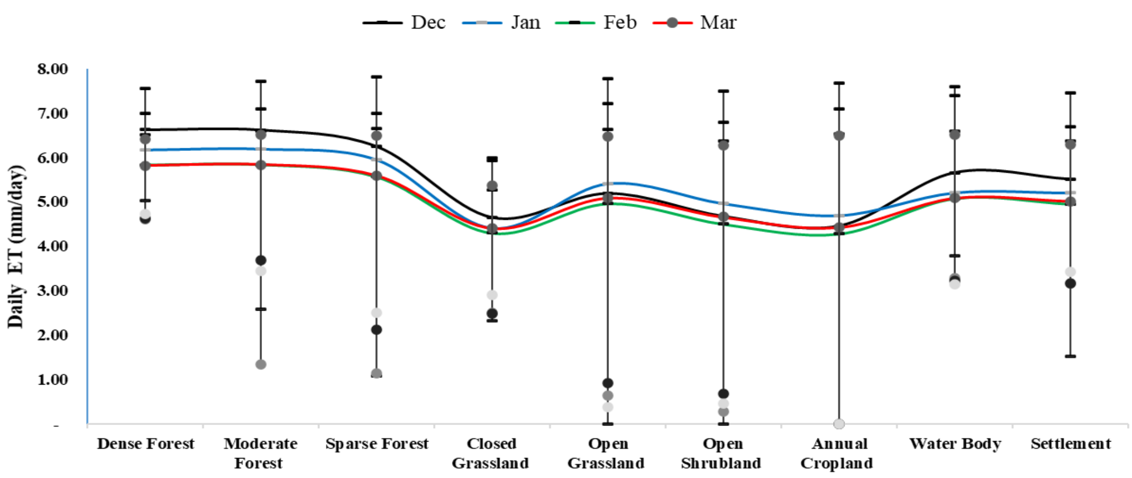

Figure 12. ET (mm/day) distribution for different land cover types in selected month.

A seasonal ET map of the study area for selected months (December to March 2016) was prepared (Fig. 13). The mean maximum ET (mm) was in forestland cover type (Table 2), but this covered a low proportion of the total study area (4.37%). The highest area coverage (88.49 km^2) produced the minimum ET (528.08 mm). The mean value of the study area was 537.92 mm for this selected four months in 2016.

The seosnal ET variation for different land cover types are presented in Figure14. ...

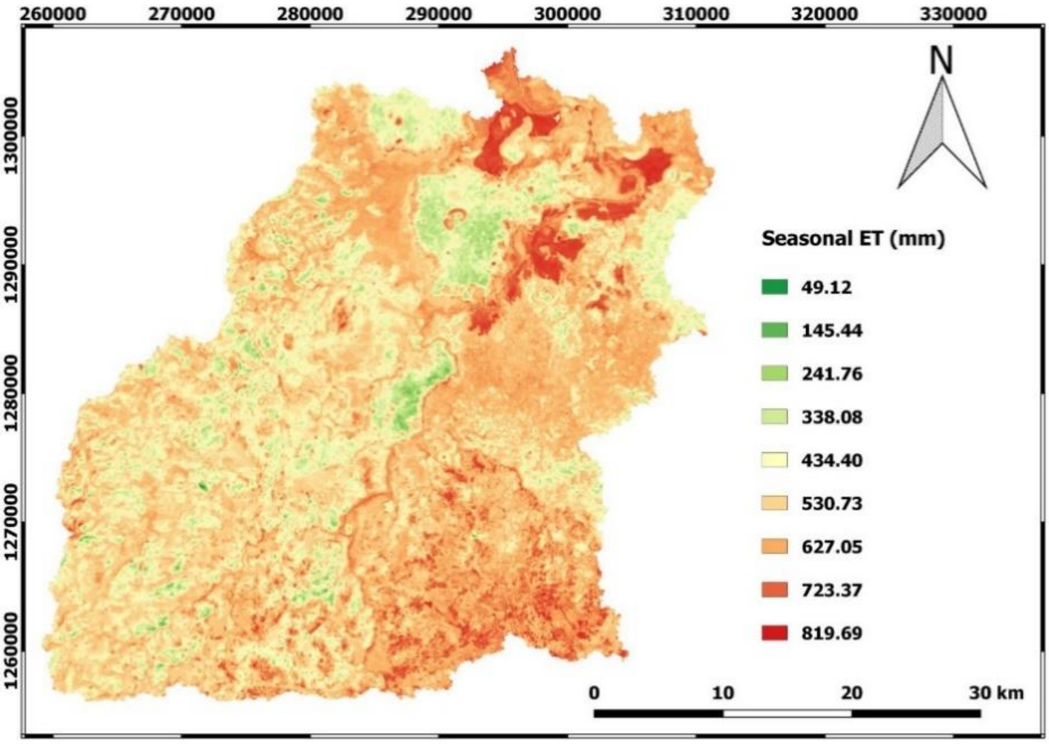

Figure 13. The combination map of ET for the selected period (Dec to Mar 2016) of the study area.

Table 2. Seasonal ET distribution and its area coverage for each land use type.

Land Cover Type	Area (km2)	%	Min ET (mm)	Max ET (mm)	Range	Mean ET (mm)	STD
Dense Forest	0.22	0.01	587.52	812.40	224.88	732.88	43.97
Moderate Forest	6.33	0.37	424.14	812.58	388.44	729.33	48.57
Sparse Forest	68.41	3.99	411.27	817.96	406.69	693.85	68.77
Closed Grassland	0.51	0.03	308.07	639.72	331.65	527.66	48.88
Open Grassland	49.43	2.88	114.77	819.69	704.92	612.09	90.21
Open Shrub land	61.67	3.60	152.77	781.97	629.19	556.12	78.25
Annual Cropland	1,516.57	88.49	49.12	804.21	755.09	528.08	95.65
Water Body	5.99	0.35	401.29	802.78	401.48	618.61	104.84
Settlement	4.72	0.28	393.08	785.80	392.71	612.76	60.42

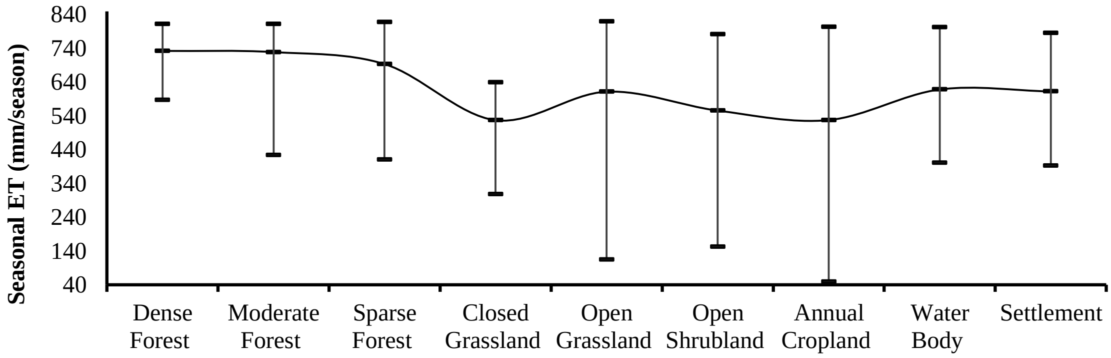

Figure 14. Seasonal ET (mm) distribution for different land cover types.

CONCLUSION

The study examined the SEBAL technique for mapping spatial variation of actual evapotranspiration over the lower part of Gilgel Abay catchment. The estimated result is based on the SEBAL method and Landsat-8 imagery at the satellite overpass time.

The majority of the land cover which mainly controlled the solar radiation and ET regime was represented by annual cropland with 88.49% of the total area, followed by sparse forest that covered about 4%, and the remaining land cover types occupied 11.51% of the total area. The daily ET map indicated that daily ET was nearly the same as the average ET in annual cropland (4.69 mm/day), higher in the forestland cover types (6.25 mm/day) and lower in closed grassland cover type (4.42 mm/day). The least range of variation in ET values was from the area characterized by the absence of vegetation cover. Hence, the variation of daily ET varied from 0 to 6.26 mm/day at the same land cover classes. The study showed a clear relation between land use/land cover and solar radiation elements and the impact of vegetation cover on the ET values in the pixel domain.

The study suggested that the SEBAL model could be applied in similar data-scarce areas at local, regional, and global scales to quantify the actual ET over various land uses and from irrigated agriculture. The spatial and temporal variation ET is a good indicator of irrigation effectiveness and total water consumption from vegetation. Evapotranspiration information from satellite imagery is useful for irrigation development and enables to improve irrigation management. It is necessary for the calculation of soil water balance, an important component of the water cycle, water rights regulation, and river basin hydrologic studies.

Among several remote sensing methods of estimating ET, the SEBAL model could be useful for irrigation water use related studies and practically applicable in the absence of ground data by providing accurate information, determine remotely over a large spatial scale, aggregated over space and time. It is user-friendly and could be widely used across a variety of climates and ecosystems. Hence, the SEBAL model is a useful tool for irrigation water use related studies.

The ET estimation using SEBAL through the use of remote sensing data is one way of estimating the evapotranspiration in a data-scare region whereby the estimation is difficult through water balance models. Moreover; with the availability of streamflow discharge measurement and with limited climate data the ET estimated using this approach could be used as a proxy in hydrological models to overcome climate data limitation in an ungauged catchment. However, the method has its own limitations including subjective specifications of representative hot/dry and wet/cool pixel selection within the image, availability of cloud-free images, lower temporal frequency but high spatial resolution imagery provided by the satellite, estimating sensible heat flux (H) which is greatly affected by the errors in surface-air temperature differences or surface temperatures measurements, and suitable to estimate ET on an hourly basis and not suitable on daily basis which could be due to the use of ETrF in extrapolating instantaneous ET to daily values. The extrapolation assumes that the ETrF at the time of satellite overpass remains constant throughout the day.

ACKNOWLEDGEMENTS
We would like to thank the Ethiopian National Meteorological Agency (ENMA) for providing weather data. The authors are grateful to the two Anonymous reviewers and the journal editor for the improvements of the manuscript.

REFERENCES

Allen, R.G. 2000. REF-ET: Reference evapotranspiration calculation software, University of Idaho, Moscow, Idaho.

Ayad, A. F., Ahmed, H. A.-S., Adrian, O., Anna, J., and Adriana, M. 2016. Estimation of Evapotranspiration Using SEBAL Algorithm and Landsat-8 Data. A Case Study: Tatra Mountains Region. *J. Geol. Res. Eng.* 6: 257-270.

Ayenew, T. 2003. Evapotranspiration estimation using thematic mapper spectral satellite data in the Ethiopian rift and adjacent highlands. *J. Hydrol.* 279: 83-93.

Bastiaanssen, W., Menenti, M., Feddes, R., and Holtslag, A. 1998. A remote sensing surface energy balance algorithm for land (SEBAL): 1. Formulation. *J. Hydrol.* 212-213: p. 198-212.

Bastiaanssen, W., Noordman, E., Pelgrum, H., Davids, G., Thoreson, B., and Allen, R. 2005. SEBAL model with remotely sensed data to improve water-resources management under actual field conditions. *J. Irrig. Drain*. 131: 85–93.

Bastiaanssen, W., Pelgrum, H., Wang, J., Ma, Y., Moreno, J., Roerink, G., and val der Wal, T. 1998. A Remote sensing surface energy balance algorithm for land (SEBAL): Part 2: Validation. *J. Hydrol.* 212: 213-229.

BCEOM. 1998. Abay River Basin Integrated Development Master Plan-Phase 2 – Data collection Site investigation survey and analysis section II Volume I (part 1 Geology). Ministry of Water Resources, Addis Ababa. 103pp.

Chiemeka, I. 2008. Estimation of solar radiation at Uturu, Nigeria. *Int. J. Physic. Sci*. 3: 26-130.

Irmak, A., Martin, D., Koelliker, J., and Eisenhauer, D. 2006a. Modeling the effects of terracing on water supplies in the Medicine Creek, Nebraska. Proc., 2006 ASABE Annual Int. Meetings, Portland, Ore., Paper No. 062291.

Irmak, S., Payero, J., Martin, D., Irmak, A., and Howell, T. 2006b. Sensitivity analyses and sensitivity coefficients of the standardized ASCE-Penman-Monteith equation to climate variables. *Irrig. Drain. Eng*. 1326: 564–578.

Jana, C., Monika, R., Sena, D., Alam, N., Mandal, U., Kaushal, R., and Mishra, P. 2016. Application of SEBAL model to estimate Evapotranspiration in Doon Valley, India. Indian *J. Soil Conserv.* 44 (2): 191-197.

Kebede, E. W. 2009. Hydrological responses to land cover changes in Gilgel Abbay catchment, Ethiopia. Master of Science in Geo-Information science and earth observation, Enschede, ITC. 80 pp.

Kosa, P. 2011. The effect of temperature on actual evapotranspiration based on Landsat-5 TM Satellite Imagery. School of Civil Engineering, Institute of Engineering, Suranaree University of Technology, INTECH Open Access Publisher, 214-215.

Lillesand, T.M., Ralph, R.W., and Chipman, J.W. 2004. Remote Sensing and Image Interpretation. Fifth Edition. John Wiley & Sons, Inc, New york. ISBN: 0-471-15227-7 .

Merlin, O., Chirouze, J., Olioso, A., Jarlan, L., Chehbouni, G., and Boulet, G. 2014. An image-based four-source surface energy balance model to estimate crop evapotranspiration from solar reflectance/thermal emission Data (SEB-4S). *Agric. For. Meteorol.* 184: 188-203.

Morse, A., Allen, R., Tasumi, M., Kramber, W., Trezza, R., and Wright, L. 2001. Application of the SEBAL methodology for estimating evapotranspiration and consumptive use of water through remote sensing. Idaho Department of Water Resources.

Muhammed, A. H. 2012. Satellite based evapotranspiration estimation and runoff simulation: a topmodel application to the gilgel abay catchment, Ethiopia. A thesis for the degree of Master of Science in Geo-information Science and Earth Observation. Enschede, The Netherlands. 85pp.

Mulugeta, G., Tena, A., Gabriel, S., and Mekonnen, G. 2017. Remote sensing based estimation of evapo-transpiration using selected algorithms: the case of Wonji Shoa Sugar Cane Estate, Ethiopia. *Int. J. Sens. Netw*. 5 (1): 1-13.

Oberg, W., and Meless, A. M. 2006. Evapotranspiration dynamics at an eco-hydrological restoration site: an energy balance and remote sensing approach. *J. Am. Water Res.. Assoc*. 42(3): 565-582.

Opoku Duah, S., Donoghue, N. M., and Burt, T. 2008. Intercomparison of Evapotranspiration over the Savannah Volta Basin in West Africa Using Remote Sensing Data. *Sensors* 8: 2736-61.

RCMRD. (2015, April 8). The Regional Centre for Mapping of Resources for Development. Retrieved from: http://geoportal.rcmrd.org

Tasumi, M., Allen, R. G., and Trezza, R. 2008. At-Surface Reflectance and Albedo from Satellite for Operational Calculation of Land Surface Energy Balance. *J. Hydrol. Eng.* 13: 51-63.

Tasumi, M., Trezza, R., Allen, R., and Wright, L. 2003. US Validation Tests on the SEBAL Model for Evapotranspiration via Satellite. In Proceedings of 54th IEC Meeting of the International Commission on Irrigation and Drainage (ICID) Workshop. Remote Sensing of ET for Large Regions. 14 pp.

Temesgen, E. 2009. Estimation of evapotranspiration from satellite remote sensing and meteorological data over the Fogera flood plain, Ethiopia. A thesis for the degree of Master of Science in Geo-information Science and Earth Observation The Netherlands 13. 101pp.

Tessema, S. M. 2006. Assessment of temporal hydrological variations due to land use changes using remote sensing/GIS: a case study of Lake Tana Basin, Master Thesis, KTH, Sweden.

Trezza, R., Allen, R., and Tasumi, M. 2013. Estimation of actual evapotranspiration along the middle Rio Grande of New Mexico using MODIS and Landsat imagery with the METRIC Model. *Remote Sens*. 5: 5397- 423.

Wagner, W. 2017. Treino GIS / SEBAL 5. Retrieved from https://www.youtube.com/watch?v=qNapB7xzB9k

Waters, R., Allen, R., Bastiaanssen, W., Tasumi, M., and Trezza, R. 2002. Surface energy balance algorithms for land. Idaho Implementation" Advanced Training and Users Manual. Idaho, USA. 98pp.

Weng, Q., Lu, D., and Schubring, J. 2004. Estimation of land surface temperature vegetation abundance relationship for urban heat island studies. *Remote Sens. Environ.* 89: 467-83.